TSUNAMI EARTHQUAKE OR ATTENUATING CRUSTAL STRUCTURE: GROUND MOTIONS FROM THE MAY 2ND, 2020, M6.6 IERAPETRA (CRETE) EARTHQUAKE

By

AVIGYAN CHATTERJEE

A THESIS

Presented to the Department of Earth Sciences
and the Division of Graduate Studies of the
University of Oregonin partial fulfillment of the requirements
for the degree of
Master of Science

June 2021

THESIS APPROVAL PAGE

Student: Avigyan Chatterjee

Title: Tsunami Earthquake or Attenuating Crustal Structure: Ground Motionsfrom the May 2nd, 2020, M6.6 Ierapetra (Crete) Earthquake

This thesis has been accepted and approved in partial fulfillment of the requirements for the Master of Science degree in the Department of Earth Sciences by:

Valerie Sahakian	Chairperson
Diego Melgar	Member
Meredith Townsend	Member

and

Andrew Karduna	Interim Vice Provost for Graduate Studies

Original approval signatures are on file with the University of Oregon Division of Graduate Studies.

Degree awarded June 2021

THESIS ABSTRACT

Avigyan Chatterjee

Master of Science

Department of Earth Sciences

June 2021

Title: Tsunami Earthquake or Attenuating Crustal Structure: Ground Motions from the May 2nd, 2020, M6.6 Ierapetra (Crete) Earthquake

Preliminary analysis of the ground-motions from the shallow M6.6 reverse-slip earthquake that struck the island of Crete on May 2nd, 2020, indicates low shaking for the earthquake's magnitude. Such behavior is common to 'Domain-A' or tsunami earthquakes according to Lay et al. 2012. Local shallow subduction zone structure and its high attenuation, due to the overlying thick accretionary wedge, could also explain the low ground motions. Analyzing the ground-motions of this earthquake will greatly help us refine our understanding of its source processes and augment our grasp over building better early warning systems. We perform a regional analysis of the ground-motions of the mainshock, its aftershocks, as well as historical seismicity, to understand whether the ground-motions we observe are due to source, or path effects. To detangle these effects, we decompose event, path, and site residuals from ground-motion models for all earthquakes in this dataset.

CURRICULUM VITAE

NAME OF AUTHOR: Avigyan Chatterjee

GRADUATE AND UNDERGRADUATE SCHOOLS ATTENDED:

University of Oregon, Eugene
Indian Institute of Science Education and Research (IISER) Kolkata, India

DEGREES AWARDED:

Master of Science, Earth Sciences, 2021, University of Oregon
BS-MS, Geological Sciences, 2019, IISER Kolkata

AREAS OF SPECIAL INTEREST:

Geophysics

PROFESSIONAL EXPERIENCE:

Teaching Assistant, University of Oregon, 1 year

GRANTS, AWARDS, AND HONORS:

First-Year-Fellowship, Doctorate Studies, University of Oregon, 2019

SSA Student Travel Award, SSA 2021, University of Oregon, 2021

ACKNOWLEDGMENTS

I sincerely thank my supervisor Dr. Valerie Sahakian for her guidance and encouragement throughout the duration of this project. The advice I received from her in this period will be treasured for the rest of my life. My committee members, Dr. Diego Melgar and Dr. Meredith Townsend, were always there by my side through thick and thin, and I cannot thank them enough for that. I also convey my gratitude to all my friends and family members who stood by my side all this time and kept faith in me when it wasn't always easy. Additionally, I thank the entire UO family for allowing me to carry out this project in such a magnificent environment. An acknowledgement would be pointless without a mention of my parents and my beloved brother. With every passing day I absolutely wonder what I did to deserve them! I haven't learnt enough words to say thanks.

To DADA,

Summers are as cold as the winter.

Winters are colder still.

I wish you were here!

TABLE OF CONTENTS

LIST OF FIGURES

Figure Page

I Introduction

Ground-motion calculations of earthquakes are a window into source processes to (a) learn more about earthquake rupture physics and tectonic processes, and (b) in the case of tsunami earthquakes, understand more about how we can improve tsunami early warning algorithms. Tsunami earthquakes are rare, end-member earthquakes that generate tsunamis much larger in size than expected for the magnitude of the event.

Not at all like most subduction zone tremors that burst profound pieces of a subduction zone, wave quakes (TsEs) break the shallowest portion (Figure 1). This district is a zone of agreeable material and was recently thought to be aseismic because of its anelastic properties; in any case, the identification of TsEs has for the most part discredited this hypothesis. Despite the fact that burst cycles of standard megathrust occasions have been altogether contemplated, the seismicity in the shallow subduction zone is as yet astounding. In any case, we do realize that cracks in this locale produce enormous removal bigger waves, and normally bring about numerous fatalities. To limit fatalities related with these uncommon occasions, it is basic to foster a strategy for separating these damaging occasions on schedule to give a torrent cautioning before immersion.

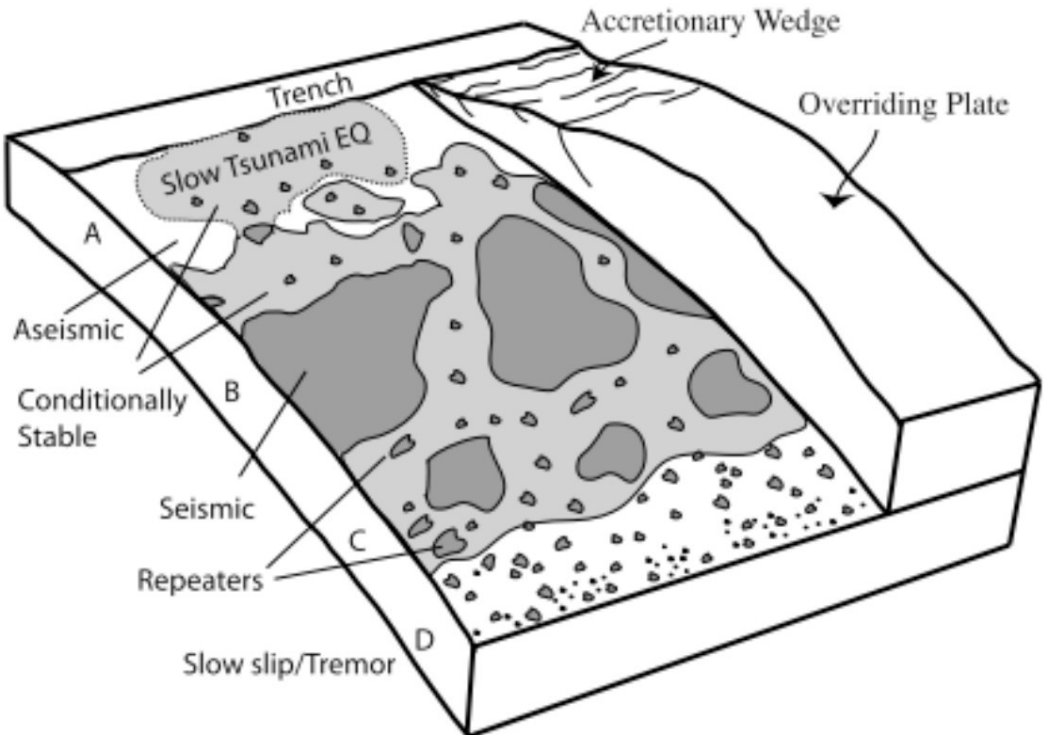

Figure 1: Illustration of subduction zone megathrust frictional properties. Tsunami earthquakes rupture in Domain A, the shallowest region overlain by the accretionary wedge. From Lay *et al.* 2012

As indicated by theoretical models (see Fig 1) of the depth-varying properties of megathrust quakes (Lay *et al.* 2012), "tsunami earthquakes" rupture the shallow-most (<10–15 km) seismogenic locale of a subduction zone (Domain A) with huge deficiency slip to the ocean bottom. Conversely, a large portion of the correspondingly estimated quakes break the plate interface at more prominent profundity inside Domains B and C. Domain A is described by consistent (Bilek & Lay 1999), fluid-rich rocks with dominatingly speed fortifying frictional properties (Faulkner *et al.* 2011) that infrequently lead to coseismic crack. At the point when an earthquake happens, rupture is slow (1.0–1.5 km/s; ammon2006rapid; lay2012depth) because of a low unbending nature, yet this doesn't hinder huge slip. Indeed, huge slip is needed to create a given second. The 2010 Mentawai tremor (Hill *et al.* 2012;

Yue *et al.* 2014) is a "tidal wave" quake. It ruptured up to 20 m in the shallow megathrust and doesn't at all break Domains B or C. Conversely, other also measured occasions burst the more profound areas, however with lower (3 m) normal slip.

Preliminary ground motion analysis (see Fig.2) of the M6.6 earthquake that struck the island of Crete on May 2nd, 2020, show that they are low for such a magnitude. Such behavior is generally portrayed by 'Domain-A' earthquakes according to lay2012depth, or tsunami earthquakes. However, low ground motion from such an event could also be a property of the path the earthquake signal traverses. This means the local earth-structure and in turn the attenuation of the place could also be a plausible reason for low ground motions. Analyzing the ground-motions from this earthquake as well as other regional earthquakes is two-fold. First, studying the rupture properties of such tsunami earthquakes will greatly help us refine our understanding of its source processes and augment our grasp over building better early warning systems. Apart from the Mentawai earthquake of 2010, this earthquake would only be the second of such events with access to near-field data. Second, if the anomalously low ground-motions are indeed a path effect instead of a source effect, this knowledge will benefit the development of improved regional ground-motion models.

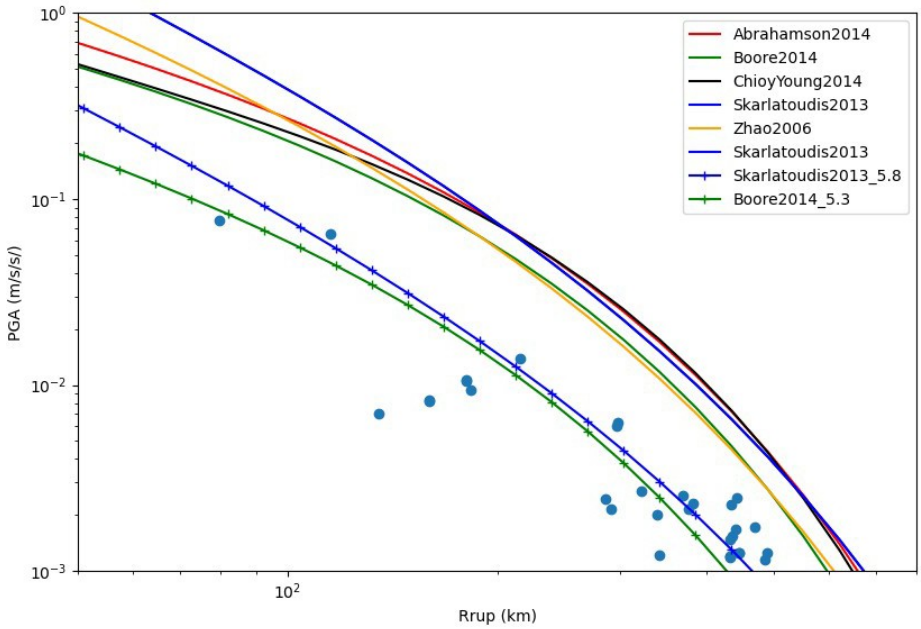

Figure 2: The strong motion data (dots below) show observed peak ground accelerations from the 2020 mainshock. The observed PGA values are compared with predicted 5 GMPEs shown in different colors. The observed PGA values for a moment magnitude of 6.6 plots really when compared to ground-motion models for a similar magnitude. For illustration purposes and to show the discrepancy, line plot with vertical dashes denoting M=5.3 for Boore, et.al, 2014 ground-motion model, and M=5.8 for Skarlatoudis, et. Al, 2013 ground-motion model, shows a better fit to the observed PGA values.

The southern Aegean structures a significant piece of the Aegean Sea plate that supersedes the subducting Nubian lithosphere in the eastern Mediterranean. The Wadati-Benioff zone studies reveal that the plunging point of the Nubian section changes from 30° in the forearc (up to 100 km profundity) to 45° in the backarc (B. C. Papazachos *et al.* 2000). The convergence between the Eurasian and the Aegean Sea plate (30 mm/yr), which is quicker than the one between the Eurasian and the Nubian plate (10 mm/yr) (Figure 3), is related with the Nubian piece rollback just as the toward the west break of the Anatolian plate limited by the North and East Anatolian flaws (Argus *et al.* 2011; Reilinger *et al.* 2006). These main impetuses have

caused expansion in the Aegean outside and brought about the arrangement of the Aegean Sea during the Oligocene-Miocene. The augmentation additionally initiated the SW movement of the volcanic circular segment, whose current position is at the southern limit of the island gathering of Cyclades.

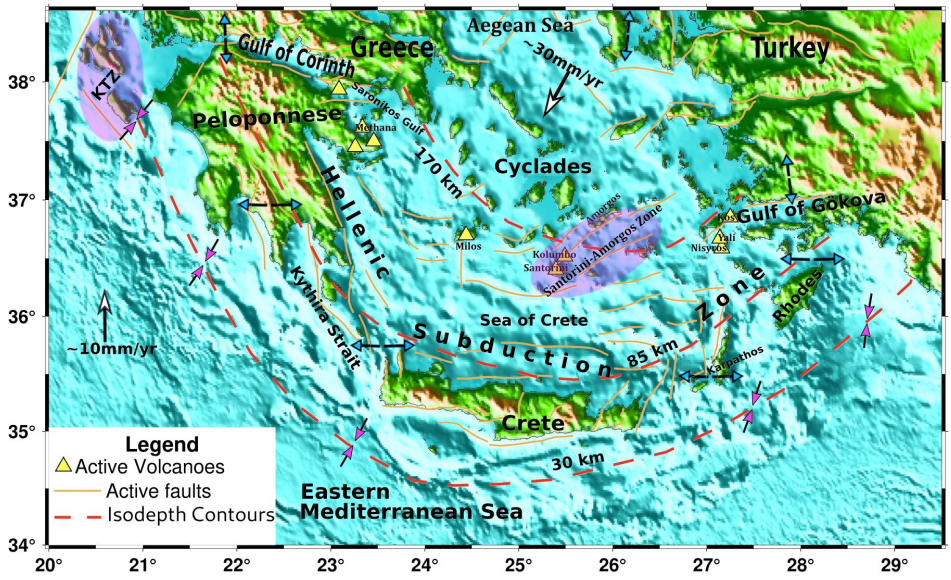

Figure 3: Map showing topographic and bathymetric features in the southern Aegean along with active faults, Benioff zone isodepth contours (B. C. Papazachos *et al.* 2000), and active volcanoes (see legend on the bottom left). The GPS velocities of the Aegean Sea plate and Nubian plate are marked with black arrows having white arrowheads (Argus *et al.* 2011). The regional stress field is shown using black arrows with blue and pink arrowheads.

The southern Aegean region is situated along an active plat boundary system (Hellenic circular segment) and has a confounded topographical and seismotectonic setting (Figure 3). Reverse faulting earthquakes are found at shallow depths (normally 30–60 km) while shallow normal faulting (in-section) earthquakes happen along a clear cut Wadati–Benioff zone at depths going from 60–170 km (B. Papazachos & Comninakis 1971; le1979hellenic). The foci of the transitional profundity seismic tremors structure two fragments of the southern Aegean–Benioff zone with various plunging points. The first shallower fragment (central profundities between around 30

and 90 km) has a lower plunging point and compares to the outside (external circular segment) part of the Benioff zone (see Fig.3), which stretches out beneath the external sedimentary Hellenic bend. The second further fragment (profundities 90–160 km) compares to the inward (internal curve) Benioff zone area (see likewise Fig.1), plunging steeply beneath the southern Aegean volcanic bend (e.g., B. Papazachos 1990; B. C. Papazachos *et al.* 2000).

The attenuation of seismic waves is a pointer of the inhomogeneous design and the anelastic conduct of the Earth. Seismic waves attenuate by two methods: first by the rearrangement of energy as it is dispersed by inhomogeneous media, known as scattering attenuation, and second by the change of seismic energy to warm, known as intrinsic attenuation (sato2012seismic). Crete demonstrates solid scattering attenuation in all recurrence groups while reasonably high intrinsic attenuation in 1–2 and 4–8 Hz groups. In view of the scattering attenuation upsides of this district, we have isolated the area into 4 sections, which is indicated by the four unique polygons. Since the attenuation esteems in these four distinct polygons are extraordinary, they assisted us with approving our cases of seismic energy rot and the subsequent low ground-movements of quakes.

To deconstruct whether these low ground-motions are a source or path effect, we compared the observed shaking of this earthquake as well as several others to predictions from ground-motion models, both global as well as regional. There are numerous measurements to earthquake hazard mitigation and risk assessment, and precisely assessing earthquake ground motion is quite possibly the main assignments. For the engineering community, ground-motion models (GMMs) are the chief methods for assessing ground motion. Notwithstanding peril risk assessments and

site-explicit investigations for building plan, GMMs are utilized in an assortment of seismological issues, including earthquake early warning systems, rapid earthquake response (e.g., ShakeMap), and approval of material science based models of ground-movement reenactment. Since they are primarily observational, even the most complete GMMs typify extensive vulnerability of both the epistemic and aleatory sorts. GMMs for tremors that happen in subduction zones are frequently significant contribution for seismic-danger investigation. Critical risk can begin from seismic tremors both along the subduction interface just as from huge occasions inside the subducting section.

Global or large-scale GMMs are regularly less exact and exact when applied on a nearby or local scale. These inconsistencies lead to enormous vulnerabilities or standard deviations in the middle ground-movement model. Enormous vulnerabilities could bring about the overprediction of key position movements at low probabilities of exceedance (Bommer & N. A. Abrahamson 2006; Stafford 2014 ;Baltay *et al.* 2017) and decrease the viability of the GMM as an experimental gauge for approval of ground-motion simulations or local seismological examinations. Nonergodic GMMs or path specific GMPEs can help ameliorate these problems (Brune 1999; Atik *et al.* 2010). These models acknowledge that ground-motion distributions are not the same in time as in space by providing a groundmotion distribution for every path of interest as opposed to the same distribution for all possible paths. This method of computing ground motions for all possible paths also helps us consider the effects of attenuation in the earth structure. For this study we have used three ground-motion models to calculate the predicted intensity measures. A regional

GMPE developed from in-slab events in the Aegean Subduction Zone (Skarlatoudis *et al.* 2013) (SK13 hereafter). abrahamson2014summary (ASK14 hereafter) developed within the PEER West 2 Project for active shallow crustal regions is used as a global groundmotion model. Lastly, we use the zhao2016ground, (Z16 hereafter) ground-motion model developed for subduction slab earthquakes in Japan using site class and simple geometric attenuation functions.

For our analysis, we decompose event, path and site residuals from ground motion models and see which residuals carry the most weight. The residuals suggest a strong path component if they are for Crete alone, low residuals from the events in the wedge through to Crete.

II Methodology

To study ground-motion residuals, we relied on strong-motion and broadband recordings for each earthquake, using observations from a federated set of networks from the local Greece and global seismological networks, that spans Greece and Turkey, network codes, HA, HI, HL and HT (Figure 4). The intensity measures we are interested in are Peak Ground Acceleration (PGA) and Spectral Accelerations (SA). The first step towards preprocessing the data was to correct for gain and pre-filter the records so that the microseismic signature is preserved. Velocity records downloaded were then corrected for baseline effects by removing the instrument response, and high pass filtered with a 20 s filter corner. The data was further differentiated with respect to time to get acceleration records. Our initial dataset contained a total of approximately 4200 seismic records across the four different polygons for $3.5 >= Mw >= 7$. We then used a Signal-to-noise-ratio cut-off threshold of 5 to trim the dataset down to approximately 2000 seismic recordings. Signal-to-noise ratio (SNR) is an important standard to measure the quality of seismic data and plays an important role in seismic data processing and interpretation. P-wave arrivals were estimated for each recording using an average shear wave velocity of 3.8 km/s taking the average depth to be 20km. With the P-arrival times estimated, we calculated the SNR value for each record for a noise duration window of 10s prior to P-wave arrival time and a 20s signal duration window post the P-wave arrival time. The average of amplitudes of seismic records were then calculated for the signal duration and noise duration windows. The ratio of amplitude average for the signal duration window to amplitude average in the noise duration window gave us the SNR value for each record.

We also made sure that we were constraining our hypocentral distances to be within 800km for each record. The 800km threshold was decided by looking at the distances over the ground-motion models used in this study would work effectively.

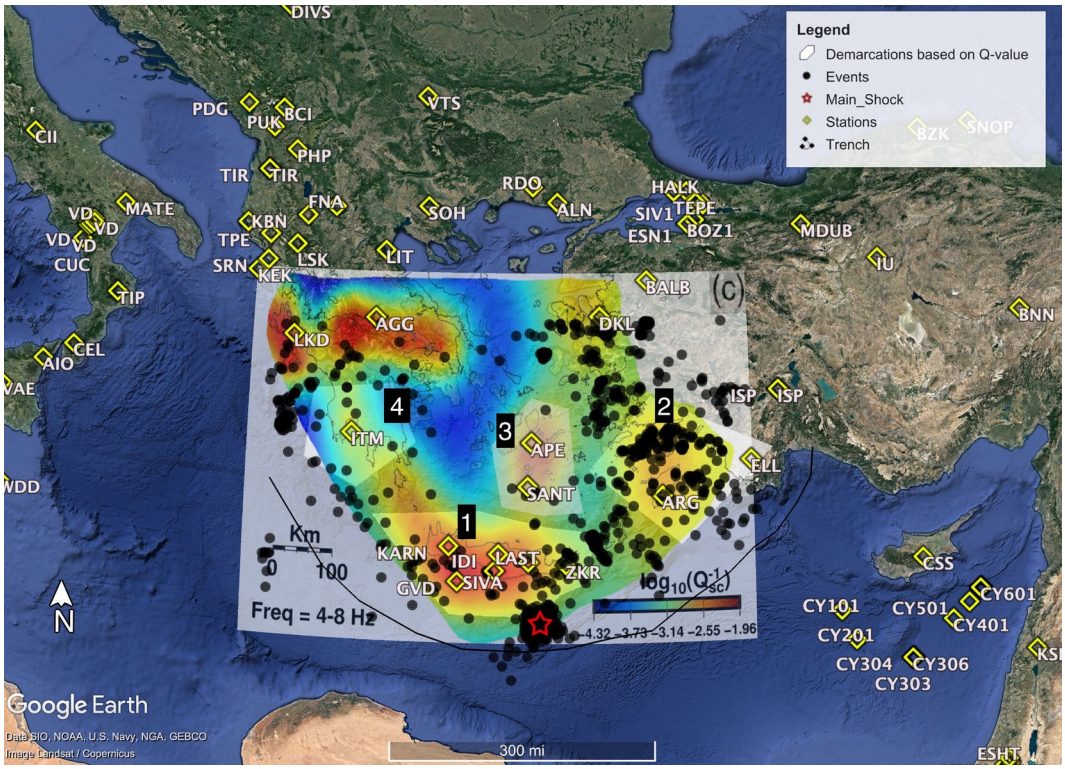

Figure 4: The area around main-shock is divided into 4 polygons (labeled in black boxes, polygons are light shaded areas) based on the value of scattering attenuation. The mainshock is plotted as a star and all other events in the polygon are plotted as black dots. The stations from the networks HA, HL, HI and HT are plotted as yellow triangles. The polygons are marked as numbers 1,2,3,4.

The two horizontal components of ground motion are combined into the orientation independent nongeometric mean (RotD50) method (Boore 2010). Using PyRotD (Kottke 2017), to compute peak ground acceleration (PGA) and the 5% damped response spectral accelerations for oscillator periods of 5.0, 4.0, 2.0, 1.0, 0.5, 0.2, and 0.1 s; we select these periods because they are common to the three GMPEs considered in this study. Peak ground Velocity was not calculated for this study because it was not common to all the three GMPEs used here.

For each record, we then compute the predicted ground-motions from a total of three ground motion models (GMMs). First, a regional GMPE developed with data from in-slab events in Greece (Skarlatoudis *et al.* 2013). SK13 reaction spectra information base is incorporated of many seismic records from intermediate-depth earthquakes (tremors whose foci are found between 45 to 300 km from the surface) with magnitude sizes of M 4.5–6.7 that happened in the South Aegean subduction zone. The data set comprises of great information from both acceleration-sensor and broadband velocity-sensor instruments

The ASK14 GMPE is an empirical ground movement models for average horizontal component from shallow crustal earthquakes in active tectonic regions are derived using the PEER NGA-West2 database. The model is pertinent to extents of magnitudes 3.0–8.5, distances 0–300 km, and spectral periods of 0–10 s. The model info boundaries are equivalent to those utilized by abrahamson2008summary, with the accompanying exemptions: the stacking level for nonlinear impacts depends on the unearthly speed increase at the time of interest instead of the PGA; and the distance scaling for hanging wall (HW) impacts off the closures of the crack remembers a reliance for the source-to-site azimuth. Territorial contrasts in enormous distance lessening and VS30 scaling between California, Japan, China, and Taiwan are incorporated.

Intended for Japan, the Z16 models foresee ground movements for interface, and insection (SSlab) occasions independently, and was created on information of distances under 300 km. They expect that each sort of occasion shows different attenuation as an element of distance. The zhao2016ground models are at present utilized by the U.S. Land Survey ShakeMap item for subduction zone settings around

the world, including the ShakeMap for the September quakes. The utilitarian structure for the Zhao *et al.* 2016 model incorporates terms addressing size scaling, geometrical spreading, intrinsic attenuation, hanging-wall effects (for crustal opposite occasions), a NEHRP site class term, central profundity, and a section versus interface order. The inslab grouping is a component of distance, to represent complex way impacts in section occasions.

All the three ground-motion models use hypocentral distance (Rhyp) for the inslab characterization, which implies the fault finite-ness of damaging inslab events can be disregarded. They chose to use hypocentral distance because the magnitude of the inslab events is not as high as that of interface events. For the main shock event, GMMs rely on closest distance to rupture (Rrup). We consider only those parts of the slip model having a minimum of 20% of the peak slip in the entire model (Figure 5).

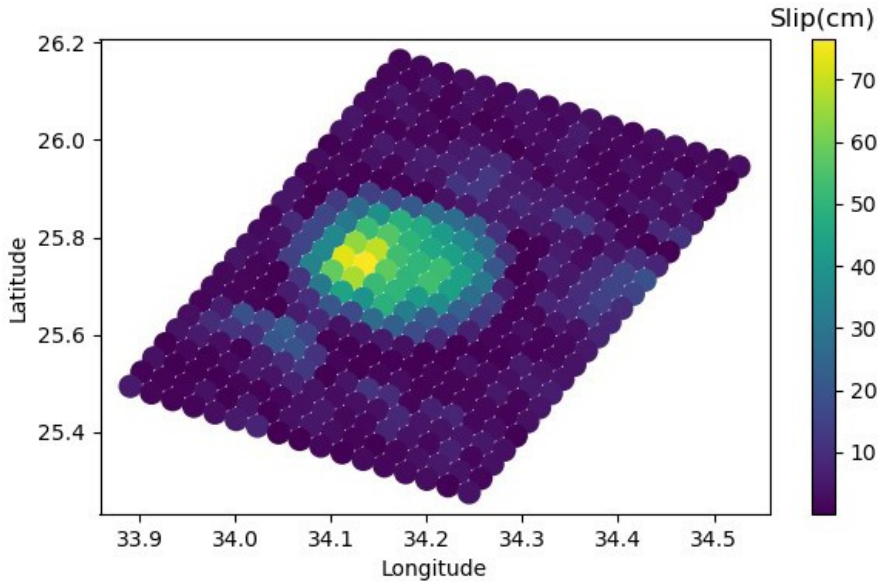

Figure 5: Slip inversion results from Tuncay, et. al (2021) (in review) for the mainshock event shows one large, concentrated patch of displacement. The Rrup for each site to the mainshock was calculated for the closest distance to the rupture where at least 20% of the slip is present.

We determine a proxy VS30 value for each site for which we have seismic data, which represents the time-averaged shear-wave velocity in the top 30 m of the surface at a station. The ASK14 and Z16 GMPEs include site terms for either nonlinear VS30 effects, or site classification dependent on VS30, which we implement. Additionally, we classify each site as either fore-arc or back-arc, for implementation into the SK13 GMPE, a distinction that is somewhat straight- forward at subduction zones with simple arc structures.

For each earthquake and GMPE, we calculate residuals between observed and predicted ground motions as,

$$\delta_{ij} = ln(Y_{ij},obs) - ln(Y_{ij},pred) \quad (1)$$

in which Y is the intensity measure (PGA, or spectral acceleration [SA]) from the GMPE for any earthquake i at station j. The total residual can be decomposed into components that represent contributions from the source (event), path, and site. It is traditionally considered to first be decomposed into δE_i, the average event-term (also called betweenevent or interevent) residual, and the within-event (or intraevent) residual δW_{ij}, for the recording of event i at station j,

$$\delta_{ij} = \delta E_i + \delta W_{ij} \quad (2)$$

The within-event residual is a combination of a site-term residual δS_j at station j, pathterm residual δP_{ij}, and the remaining random residual for recording of earthquake i at station j, δW_{0ij}:

$$\delta W_{ij} = \delta S_j + \delta P_{ij} + \delta W_{0ij} \quad (3)$$

Because we cannot separate out the path residual from random residual δW_{0ij}, we combine them to be δW_{ij} and hereafter call this the path term or path residual, using the same notation as Baltay et al. (2017). We have additionally introduced another term called the polygon residual term δPol, to account for the residual inside each polygon. Hence Eq.4 is rewritten as,

$$\delta W_{ij} = \delta S_j + \delta P_{ij} + \delta Pol + \delta W_{0ij} \quad (4)$$

We did perform a mixed-effects regression with a bias term to investigate between-event (event-term), within-event (station- term) residuals and within-polygon (polygon-term) residuals. A MLE or REML mixed-effects model will allow both the GMPE coefficients and event and site terms to be inverted for simultaneously, as well as all their respective uncertainties. In this model, all of the GMPE coefficients are considered fixed effects because their relation- ship to the predictive parameter is constant regardless of the selected population of data. The selected populations of events and sites, however, will affect the uncertainty of the model differently with every population.

III Results

Observed and predicted intensity measures, PGA and SA were calculated for the main shock and all the other recordings for each polygon. The residuals were calculated similarly for each recording. The residuals were decomposed to find the event, site, and path residuals. Since we have also introduced the polygon residuals term, we are representing the event residuals to be a combination of event plus polygon residuals.

3.1 Mainshock

The observed PGA values for the M6.6 mainshock was very low. When plotted against the three ground-motion models, ASK14, SK13 and Z16, the ground-motions are particularly low for PGA and the higher frequencies.

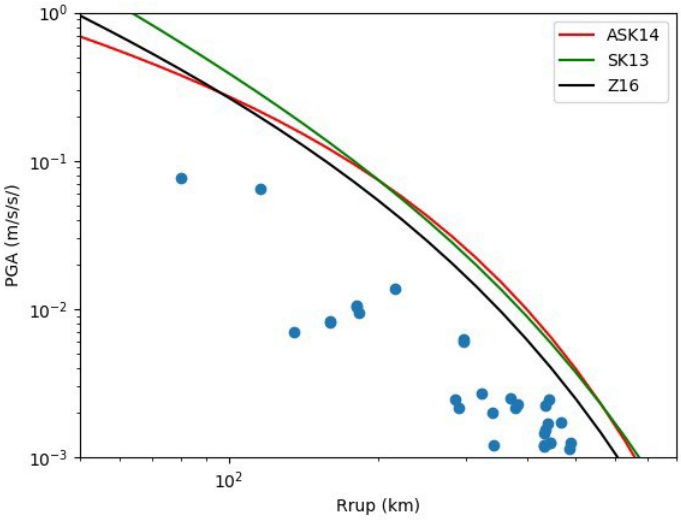

(a)

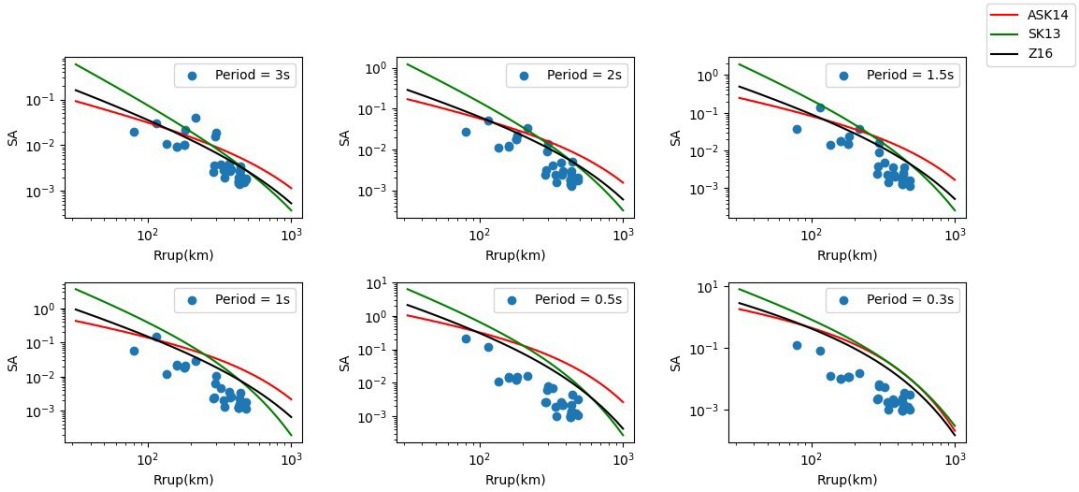

(b)

Figure 6: The observed PGA and SA values for the mainshock plotted with predicted values from the three ground motion models.

3.2 Polygon 1

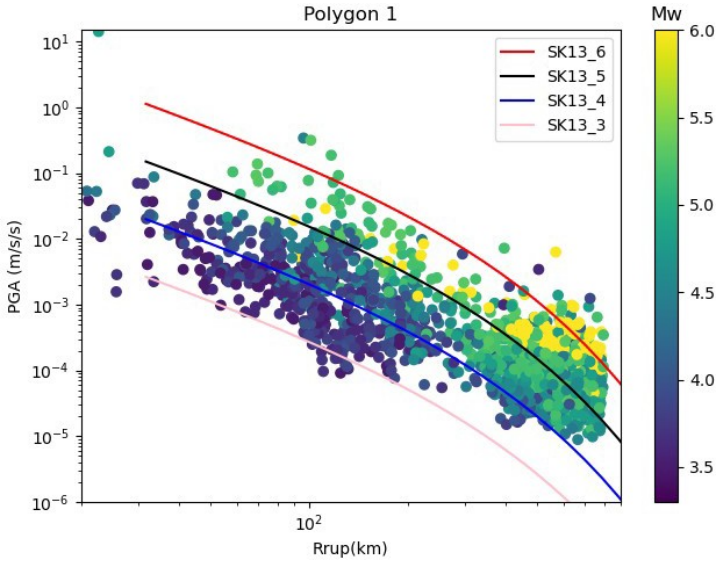

(a)

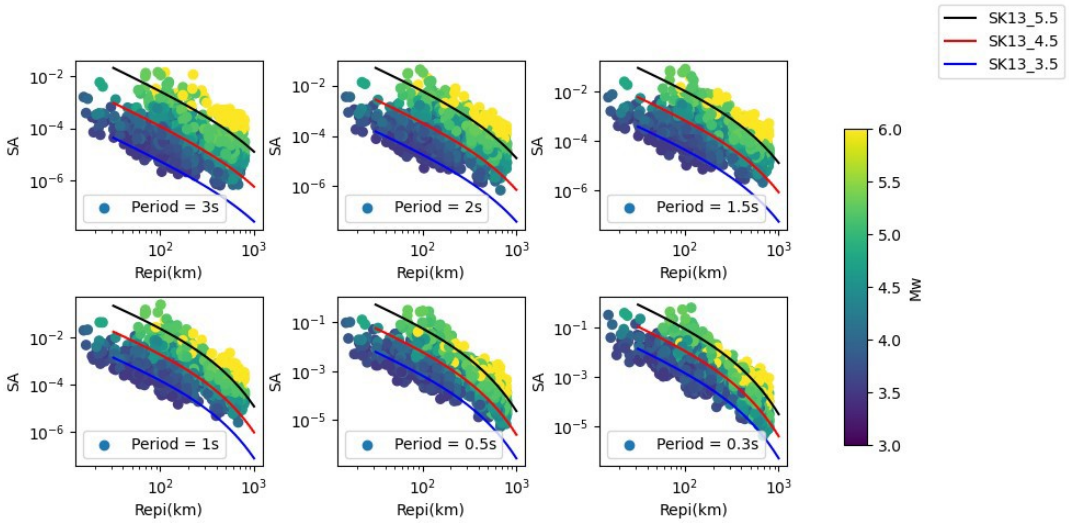

(b)

Figure 7: The observed PGA and SA values for events in polygon 1 plotted with predicted values from only the local ground-motion model, SK13.

3.3 Polygon 2

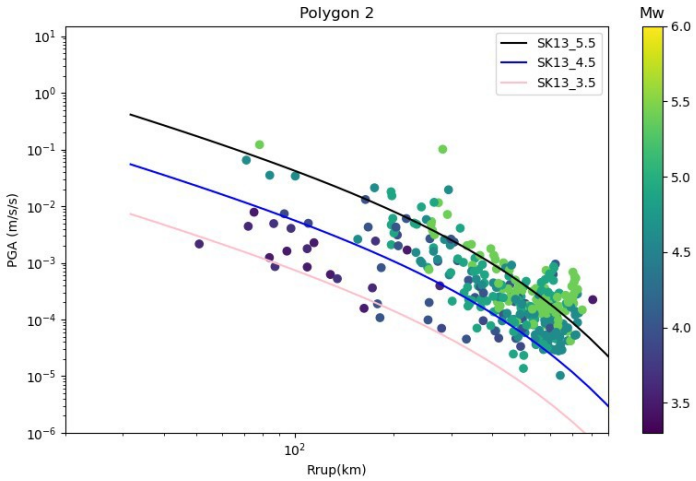

(a)

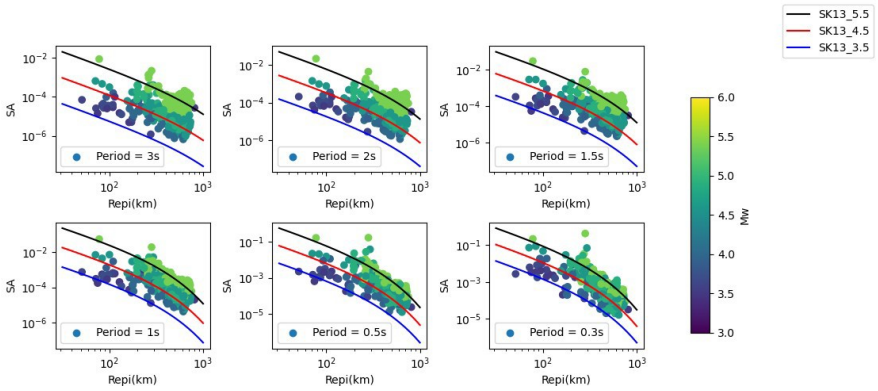

(b)

Figure 8: The observed PGA and SA values for events in polygon 2 plotted with predicted values from only the local ground-motion model, SK13.

3.4 Polygon 3

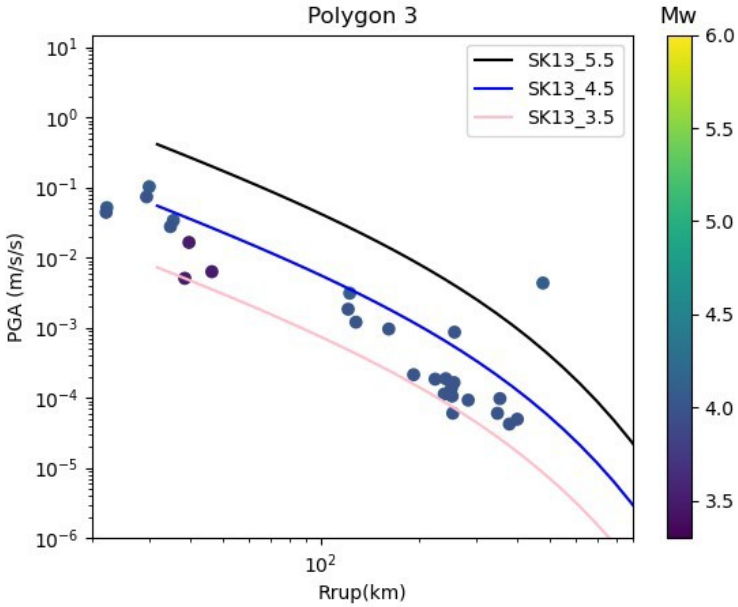

(a)

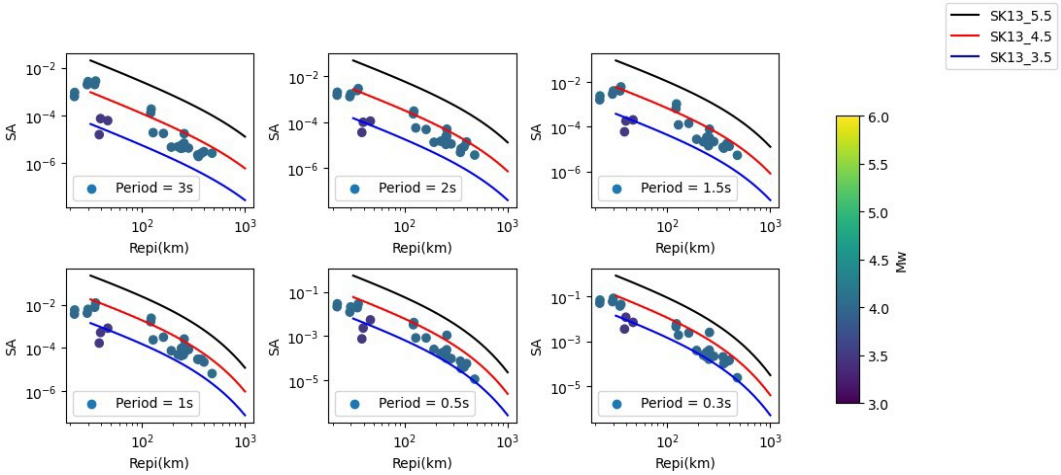

(b)

Figure 9: The observed PGA and SA values for events in polygon 3 plotted with predicted values from only the local ground-motion model, SK13.

3.5 Polygon 4

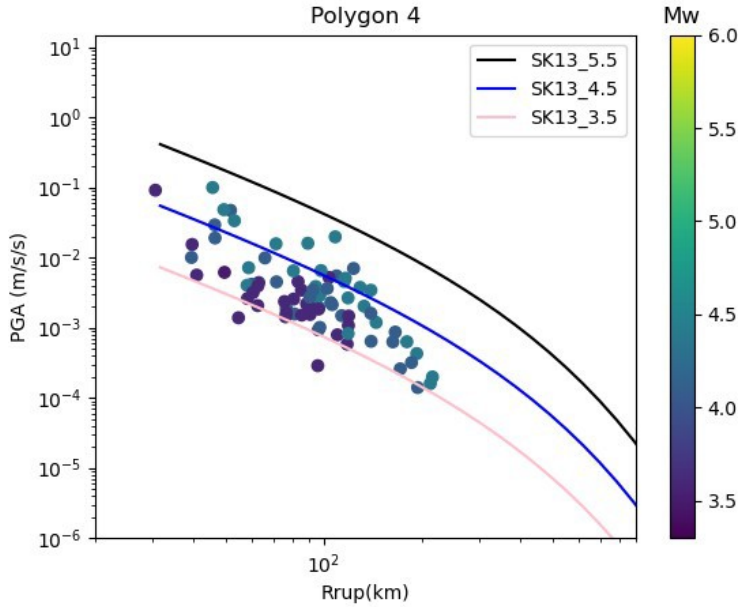

(a)

(b)

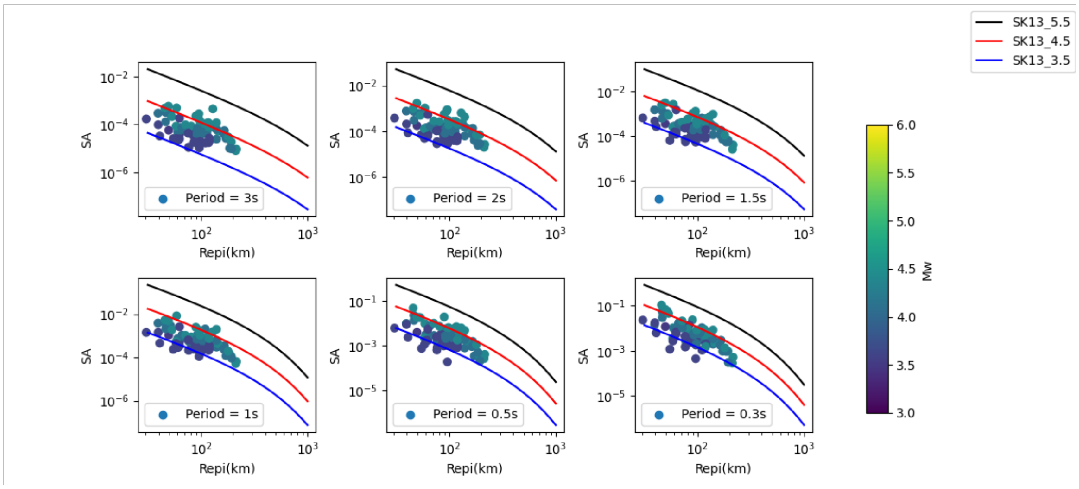

Figure 10: The observed PGA and SA values for events in polygon 4 plotted with predicted values from only the local ground-motion model, SK13.

IV Discussion

To find the reason behind the low PGA values of the main shock, we had segregated the region around the island of Crete into 4 zones, marked by the polygons. These polygons were drawn keeping in mind how the scattering attenuation in the region changes. Intensity measures, namely PGA and SA for events recorded in these four distinct areas were calculated to seek answers to this question of low ground motions. The computed PGA and SA values were compared against the three ground-motion models to calculate the residuals. The residuals were further decomposed to find event, site and path residuals.

The residuals for the main-shock were significantly low as is shown in Figure 11. The REML algorithm does not allow for decomposition of a single event.

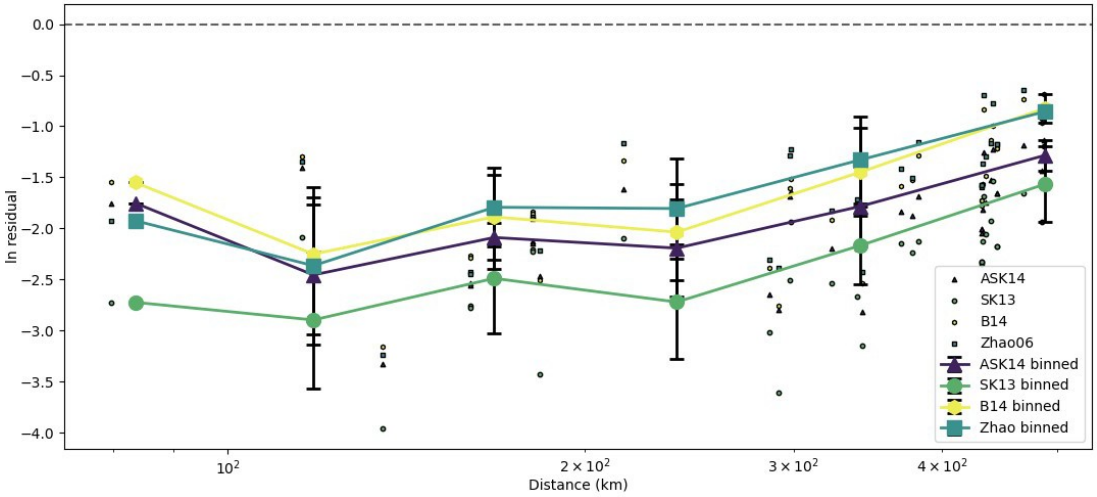

Figure 11: The natural log of residuals for the main shock plotted against the Rrup.

However, when the residuals for the events in the rest of the polygons were plotted, the residuals for polygon 1 were the lowest followed by polygon 4. This can be attributed to the fact that the scattering attenuation value is high in these two areas,

with the area enclosed by polygon 1 having the highest attenuation value in the region. The residuals were polygon 2 and 3, were mostly centered around the zero line (Figure 12). It must also be noted that the Z16 model does not perform well when compared to the ASK14 and SK13 models. This could be because the Z16 GMPE was developed from events that occurred in the Japan subduction zone. Subduction zone properties vastly vary across different tectonic settings.

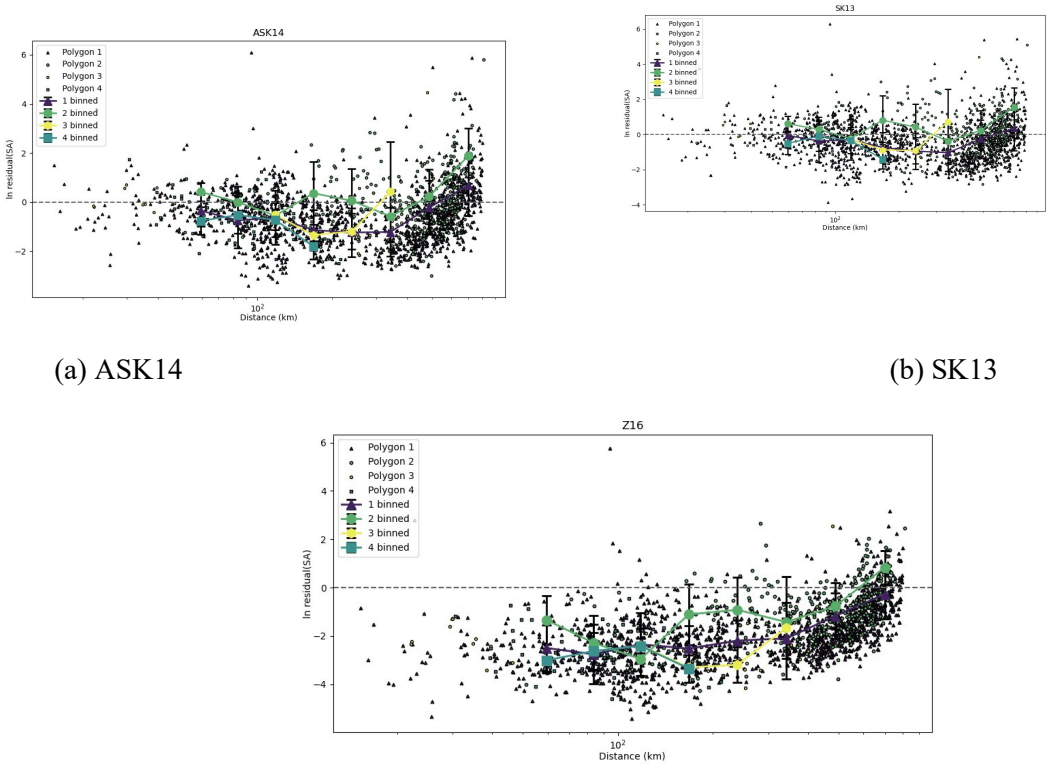

(a) ASK14

(b) SK13

(c) Z16

Figure 12: Comparison of total residuals for all the four polygons across the three different ground-motion models.

The event plus polygon residuals seem to suggest that although the events show some lower source properties along the front of the wedge overall, the smaller section near the mainshock shows even lower event residuals, suggesting there may

additionally be some component of a source effect to the low ground-motions in this area which warrants further exploration. Again, the Z16 model fares the worst amongst the three (Figure 13).

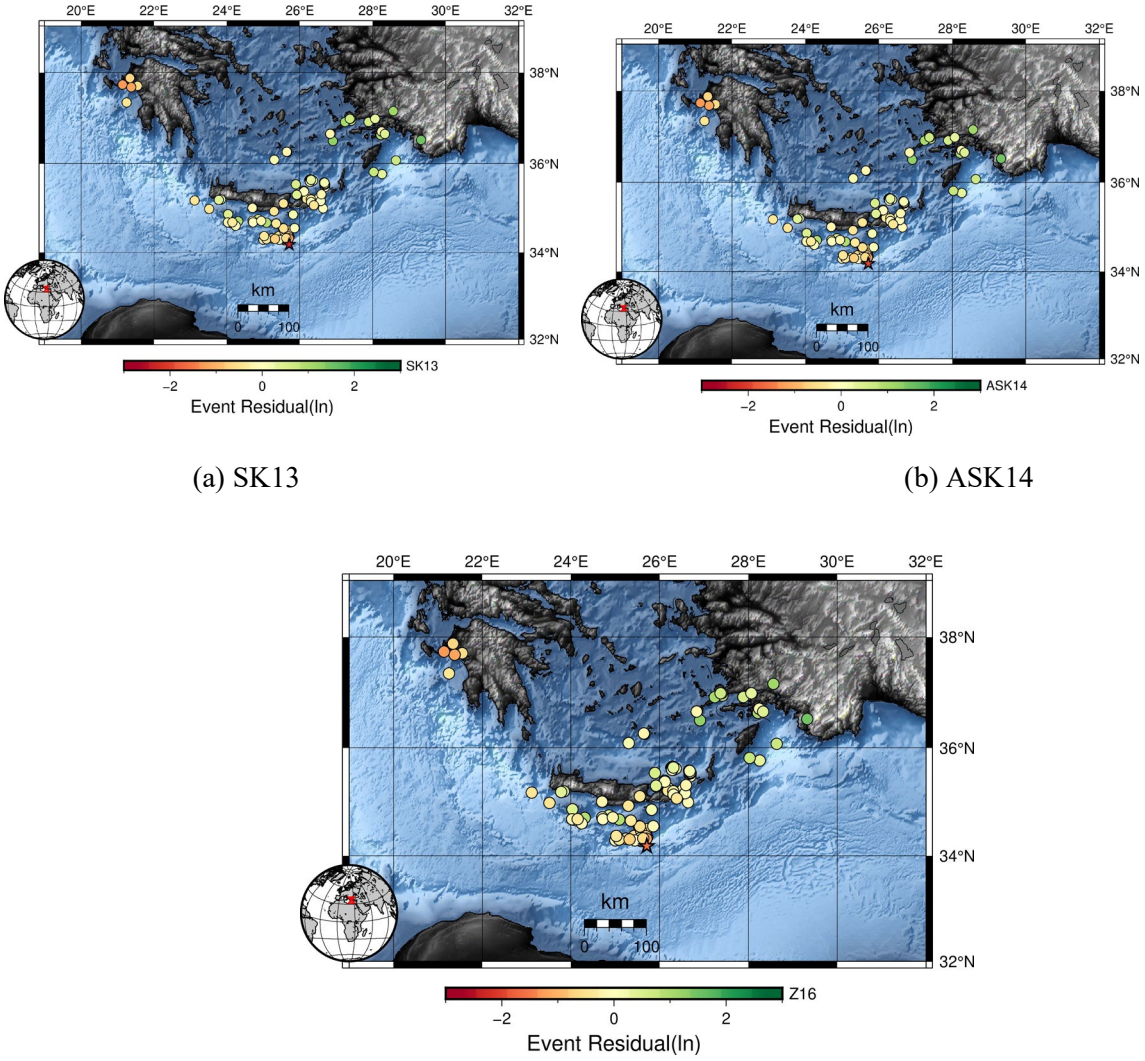

(a) SK13

(b) ASK14

(c) Z16

Figure 13: Map view of event plus polygon residuals. The area near the wedge shows consistently low event plus polygon residuals. The star in the map denotes the mainshock and is color coded according to its mean total residual.

The station site residuals show that the stations that fall in the forearc of the subduction zone have consistently low residuals compared to those in the backarc.

This is a known phenomenon and can be attributed to factors like the waveguide effect in subduction zones(Figure 14).

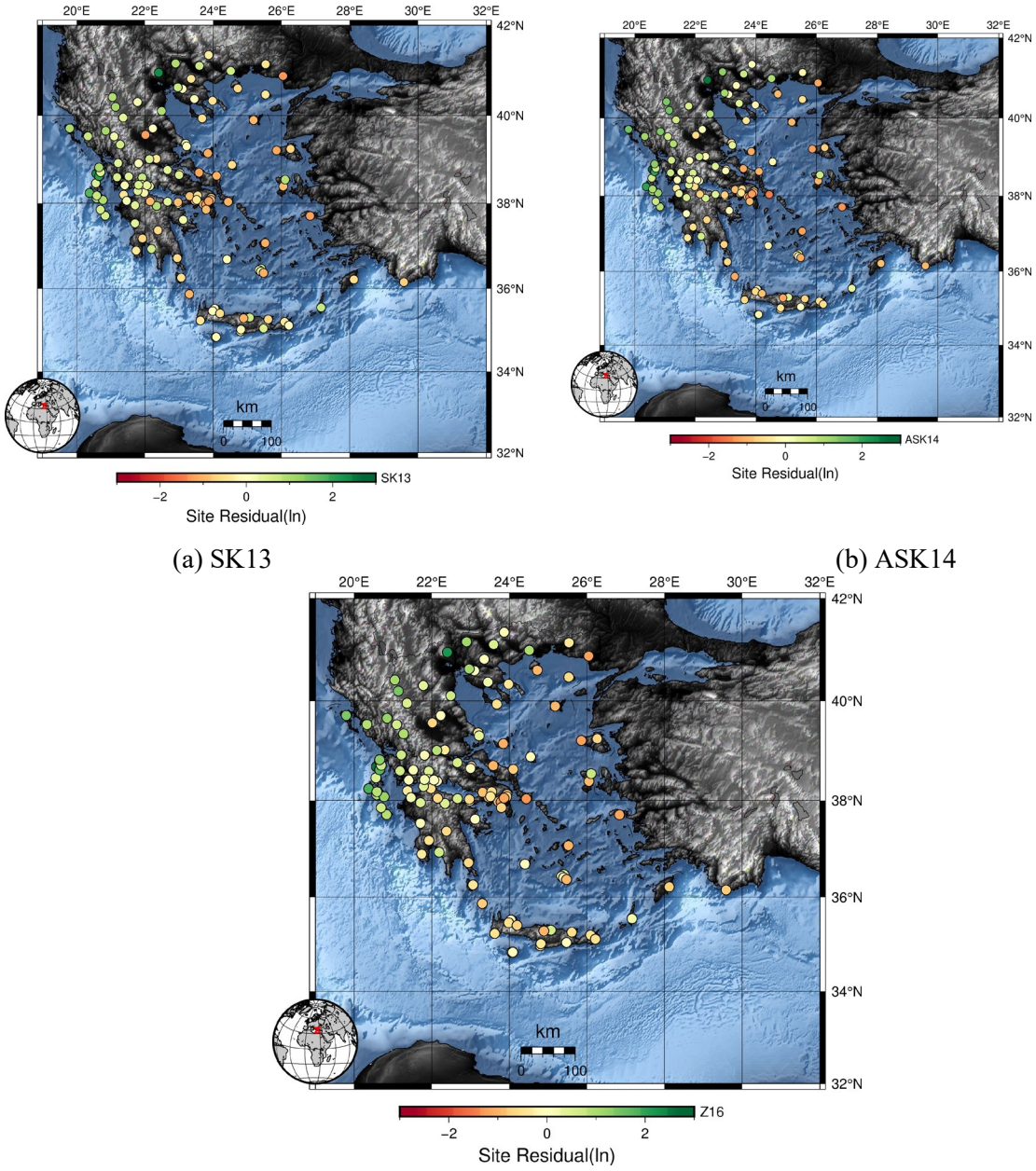

(a) SK13

(b) ASK14

(c) Z16

Figure 14: The site residuals showing lower residuals in the forearc area of the subduction zone region.

The path residuals suggest that there is an identifiable a path component to lower ground-motions if they are recorded on Crete alone, really low path residuals from the events in the wedge through to Crete (Figure 15). The path residuals for each polygon from the

SK13 model calculated is shown here. The other models are not shown because the SK13 model is the only model used in this study that incorporates the effects of arc structure in the subduction zone.

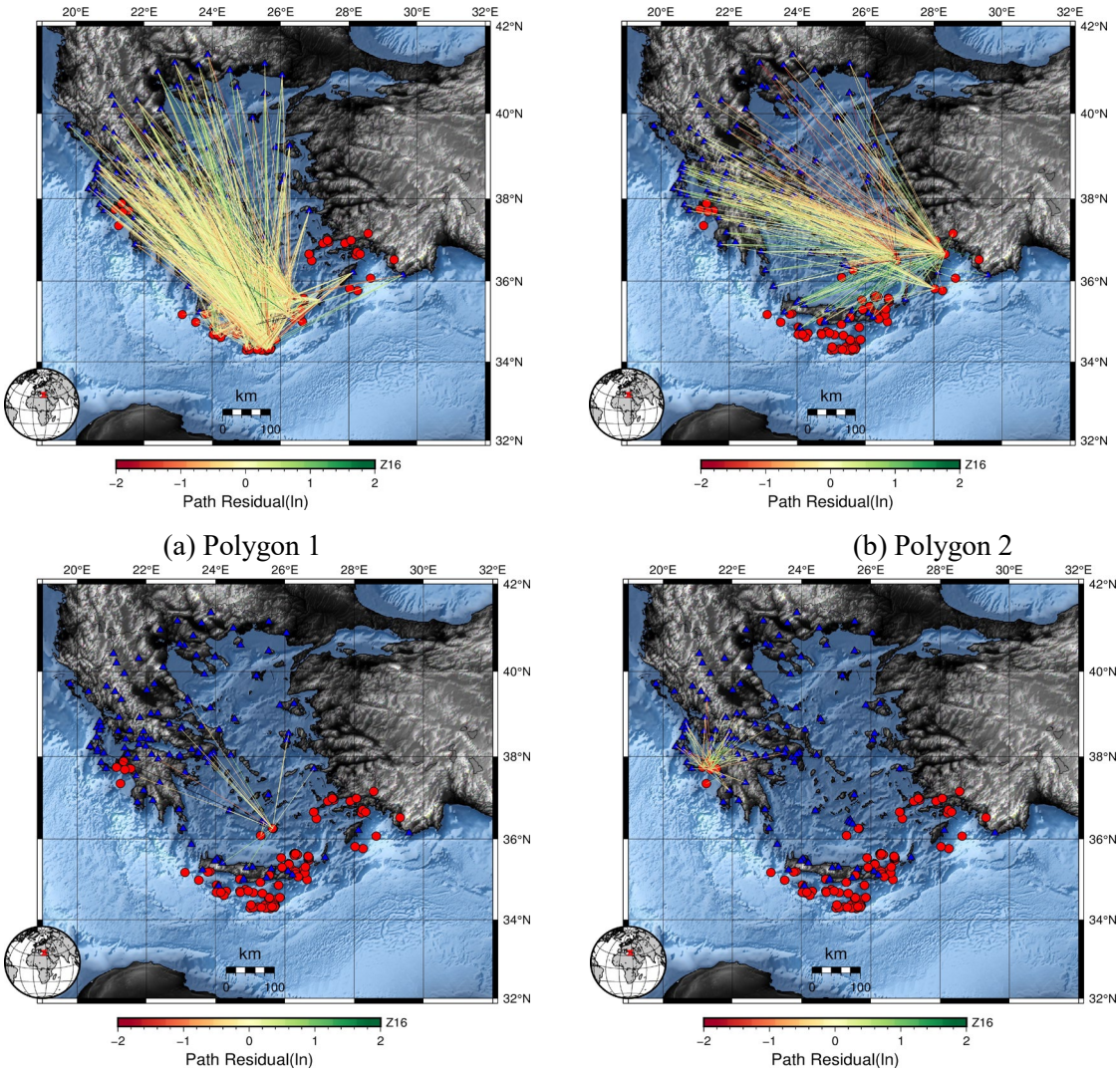

(a) Polygon 1

(b) Polygon 2

(c) Polygon 3

(d) Polygon 4

Figure 15: The event to site raypaths are color coded according to the path residual for each recording.

V Conclusion

We analyze ground-motion recordings from the 2020 M6.6 Crete mainshock, and decompose ground-motion residuals from three GMMs into regional, event, site, and path terms. We find that seismic energy traversing the accretionary wedge shows a depletion in energy, mostly for the periods greater than 2s, more so than events traversing other regions. However, we also find that events very close to the mainshock location show lower than normal event residuals, suggesting that there is some component of energy depletion due to source properties of the mainshock, and not just path properties. This is evident from the total residual plots for each polygon. Polygon 1 has consistently lower residuals compared to the other polygons. Path and source properties around the wedge warrant additional exploration in this area.

REFERENCES CITED

1. Abrahamson, N. & Silva, W. Summary of the Abrahamson & Silva NGA Ground-Motion Relations. *Earthquake spectra* **24,** 67–97 (2008).

2. Abrahamson, N. A., Silva, W. J. & Kamai, R. Summary of the ASK14 Ground Motion Relation for Active Crustal Regions. *Earthquake Spectra* **30,** 1025–1055 (2014).

3. Ammon, C. J., Velasco, A. A. & Lay, T. Rapid Estimation of First-Order Rupture Characteristics for Large Earthquakes Using Surface Waves: 2004 Sumatra-Andaman Earthquake. *Geophysical research letters* **33** (2006).

4. Argus, D. F., Gordon, R. G. & DeMets, C. Geologically Current Motion of 56 Plates Relative to the No-Net-Rotation Reference Frame. *Geochemistry, Geophysics, Geosystems* **12** (2011).

5. Atik, L. A. *et al.* The Variability of Ground-Motion Prediction Models and Its Components. *Seismological Research Letters* **81,** 794–801 (2010).

6. Baltay, A. S., Hanks, T. C. & Abrahamson, N. A. Uncertainty, Variability, and Earthquake Physics in Ground-Motion Prediction Equations. *Bulletin of the Seismological Society of America* **107,** 1754–1772 (2017).

7. Bilek, S. L. & Lay, T. Rigidity Variations with Depth along Interplate Megathrust Faults in Subduction Zones. *Nature* **400,** 443–446 (1999).

8. Bommer, J. J. & Abrahamson, N. A. Why Do Modern Probabilistic Seismic-Hazard Analyses Often Lead to Increased Hazard Estimates? *Bulletin of the Seismological Society of America* **96,** 1967–1977. issn: 0037-1106 (Dec. 1, 2006).

9. Boore, D. M. Orientation-Independent, Nongeometric-Mean Measures of Seismic Intensity from Two Horizontal Components of Motion. *Bulletin of the Seismological Society of America* **100,** 1830–1835 (2010).

10. Brune, J. N. Precarious Rocks along the Mojave Section of the San Andreas Fault, California: Constraints on Ground Motion from Great Earthquakes. *Seismological Research Letters* **70,** 29–33 (1999).

11. Faulkner, D., Mitchell, T., Behnsen, J., Hirose, T. & Shimamoto, T. Stuck in the Mud? Earthquake Nucleation and Propagation through Accretionary Forearcs. *Geophysical Research Letters* **38** (2011).

12. Hancock, J. *et al.* An Improved Method of Matching Response Spectra of Recorded Earthquake Ground Motion Using Wavelets. *Journal of earthquake engineering* **10,** 67–89 (spec01 2006).

13. Hill, E. M. *et al.* The 2010 Mw 7.8 Mentawai Earthquake: Very Shallow Source of a Rare Tsunami Earthquake Determined from Tsunami Field Survey and near-Field GPS Data. *Journal of Geophysical Research: Solid Earth* **117** (2012).

14. Kottke, A. *VS30–K0 Relationship Implied by Ground Motion Models?* in *16th World Conference on Earthquake Engineering (16WCEE)* (2017).

15. Lay, T. *et al.* Depth-Varying Rupture Properties of Subduction Zone Megathrust Faults. *Journal of Geophysical Research: Solid Earth* **117** (2012).

16. Le Pichon, X. & Angelier, J. The Hellenic Arc and Trench System: A Key to the Neotectonic Evolution of the Eastern Mediterranean Area. *Tectonophysics* **60,** 1–42 (1979).

17. Papazachos, B. C., Karakostas, V., Papazachos, C. & Scordilis, E. The Geometry of the Wadati–Benioff Zone and Lithospheric Kinematics in the Hellenic Arc. *Tectonophysics* **319,** 275–300 (2000).

18. Papazachos, B. Seismicity of the Aegean and Surrounding Area. *Tectonophysics* **178,** 287–308 (1990).

19. Papazachos, B. & Comninakis, P. Geophysical and Tectonic Features of the Aegean Arc. *Journal of Geophysical Research* **76,** 8517–8533 (1971).

20. Reilinger, R. *et al.* GPS Constraints on Continental Deformation in the Africa Arabia-Eurasia Continental Collision Zone and Implications for the Dynamics of Plate Interactions. *Journal of Geophysical Research: Solid Earth* **111** (2006).

21. Sato, H., Fehler, M. C. & Maeda, T. *Seismic Wave Propagation and Scattering in the Heterogeneous Earth* (Springer, 2012).

22. Skarlatoudis, A. *et al.* Ground-Motion Prediction Equations of Intermediate-Depth Earthquakes in the Hellenic Arc, Southern Aegean Subduction Area. *Bulletin of the Seismological Society of America* **103,** 1952–1968 (2013).

23. Stafford, P. J. Crossed and Nested Mixed-Effects Approaches for Enhanced Model Development and Removal of the Ergodic Assumption in Empirical Ground-Motion Models. *Bulletin of the Seismological Society of America* **104,** 702–719 (2014).

24. Yue, H. *et al.* Rupture Process of the 2010 Mw 7.8 Mentawai Tsunami Earthquake from Joint Inversion of near-Field Hr-GPS and Teleseismic Body Wave Recordings Constrained by Tsunami Observations. *Journal of Geophysical Research: Solid Earth* **119,** 5574–5593 (2014).

25. Zhao, J. X. *et al.* Ground-Motion Prediction Equations for Subduction Slab Earthquakes in Japan Using Site Class and Simple Geometric Attenuation Functions. *Bulletin of the Seismological Society of America* **106,** 1535–1551 (2016).